Coherent Elastic Neutrino-Nucleus Scattering in the Standard Model and Beyond

Valentina De Romeri

Instituto de Física Corpuscular, CSIC-Universitat de València, 46980 Paterna, Spain

Abstract

I will present the physics potential of the coherent elastic neutrino-nucleus scattering (CEνNS) process. I will first briefly review the status of current observations. Then, I will comment on their implications for both precision tests of the Standard Model and for new physics in the neutrino sector. Finally, I will discuss the relevance of these measurements for direct dark matter detection probes.

Keywords: neutrinos, CEνNS, neutrino floor, dark matter
DOI: 10.31526/LHEP.2023.343

1. INTRODUCTION

Coherent elastic neutrino-nucleus scattering (CEνNS) is a neutral-current process in which neutrinos scatter on a nucleus seeing it as a whole. In the Standard Model (SM), this occurs via the exchange of a Z boson. The CEνNS process arises when the momentum transfer in the neutrino-nucleus interaction is smaller than the inverse of the size of the nucleus: $|\vec{q}| \lesssim 1/\mathrm{R}_{\mathrm{nucleus}}$. The incoming neutrino energy E_ν is such that the nucleon amplitudes sum up coherently, thus leading to a cross section enhancement: $\sigma_{\mathrm{CE}\nu\mathrm{NS}} \sim \#\,\text{scatter targets}^2$. The upper limit on E_ν depends on the material of the target, but it is approximately $E_\nu \sim 100\,\mathrm{MeV}$ for typical heavy nuclei used in CEνNS detectors. Due to the nature of SM couplings, the CEνNS differential cross section turns out to scale with the number of neutrons squared: $\frac{d\sigma_{\mathrm{CE}\nu\mathrm{NS}}}{dE_r} \sim N^2$ (E_r being the recoil energy), and it can be quite sizeable. In particular, it is about two orders of magnitude larger than the inverse beta decay one, a process that was used to first observe neutrinos.

The CEνNS process was first theoretically proposed in the 1970s [1, 2]; however it eluded detection for more than 40 years for being an exceptionally challenging process to observe. Indeed, despite the magnitude of its cross section, it was not observed for years due to the tiny nuclear recoil energies produced in the scattering. The advancements in detector technologies, also related to dark matter (DM) direct detection experiments, have made this observation possible in 2017.

In 2017, the COHERENT collaboration announced the detection of CEνNS [3] using a stopped-pion source with CsI detectors. In 2021, they have released updated data [4] using the same CsI detector, and meanwhile, in 2020 they observed the process also using an Ar target [5]. The COHERENT experiment uses neutrinos from the Spallation Neutron Source (SNS). A proton beam hits a mercury target and produces π^+ and π^-. Most of the negatively charged pions are captured by nuclei, whereas the π^+ lose energy and decay at rest (DAR), $\pi^+ \to \mu^+\nu_\mu$, thus producing monoenergetic muon neutrinos. From the subsequent decay of μ^+ at rest, $\bar{\nu}_\mu$ and ν_e are also produced with some delay. More recently, in 2022, the Dresden-II collaboration [6, 7] has reported suggestive evidence pointing to what would be the first-ever observation of CEνNS with reactor antineutrinos, using a 2.924 kg ultralow noise p-type point contact germanium detector (NCC-1701). This experiment is located 10.39 meters away from the Dresden-II boiling water reactor and collected beam-ON data for a total time of 96.4 days, operating with a very low energy threshold. This result is, however, strongly dependent on the quenching factor (QF) model, one of the main sources of uncertainties for detecting facilities exploiting the ionization or scintillation generated by particle interactions.

Going back to the CEνNS theory, its cross section is well-calculable in the SM. In full generality, it would receive both vector and axial-vector contributions:

$$\begin{aligned}\left.\frac{d\sigma}{dE_r}\right|_{\mathrm{SM}} = &\frac{G_F^2 m_N}{4\pi}\left(1-\frac{m_N E_r}{2E_\nu^2}-\frac{E_r}{E_\nu}\right)Q_V^2 F_{\mathrm{W}}\left(|\vec{q}|^2\right)^2 \\ &+\frac{G_F^2 m_N}{4\pi}\left(1+\frac{m_N E_r}{2E_\nu^2}-\frac{E_r}{E_\nu}\right)F_A\left(|\vec{q}|^2\right),\end{aligned} \tag{1}$$

where G_F is Fermi's constant and m_N is the nuclear mass. The SM weak charge, Q_V, reads

$$Q_V = \left[1/2\left(1-4\sin^2\theta_W\right)\right]Z - 1/2N. \tag{2}$$

Given the value of the weak mixing angle ($\sin^2\theta_W \sim 0.23$), it eventually encodes the typical N^2 dependence. The weak nuclear form factor F_W depends on the nuclear density distribution of protons and neutrons, and it is approximated to 1 in the full-coherence limit $|\vec{q}| \to 0$. While the vector operator gives rise to the coherent contribution $\sim N^2$, the axial-vector contribution is small for most nuclei, as it adds an additional contribution that is not coherently enhanced. Moreover, it vanishes for nuclei with an even number of protons and neutrons. Therefore, it can be safely neglected.

2. PHYSICS POTENTIAL OF CEνNS

The detection of CEνNS by COHERENT and the Dresden-II suggestive evidence have opened the window to a plethora of possibilities in high-energy physics, from tests of the SM to inspiring new constraints on beyond the Standard Model (BSM) physics. Indeed, the CEνNS process has important implications not only for high-energy physics but also for astrophysics and nuclear physics.

The observation of CEνNS can provide important nuclear structure information through the determination of the weak nuclear form factor F_W, leading to a determination of the weak mixing angle at low momentum transfer, the neutron density distribution, and consequently the neutron radius and the neutron skin. Detectors sensitive to CEνNS can also play an important role in extracting information from supernova, solar, and geoneutrinos.

By means of exploiting both terrestrial (π-DAR and reactor) and astrophysical sources, the CEνNS process has the potential to probe also BSM physics. Some of the physics scenarios that can be probed are those that include new interactions in the neutrino sector, like neutrino non-standard interactions (NSI) or generalized neutrino interactions (NGI), sterile neutrinos, and nontrivial neutrino electromagnetic properties. Moreover, CEνNS constitutes a background for direct DM searches. In the following, we will discuss a few examples. (For a recent review of the topic including an extensive list of references, see [8].)

2.1. SM Precision Tests: The Weak Mixing Angle

CEνNS data allow for a determination of the weak mixing angle value at low energies, in a region where data-driven constraints were absent. A sizeable deviation from the SM expected value would be a clear hint for the existence of new physics. Figure 1 shows the $\Delta\chi^2$ profile of $\sin^2\theta_W$ obtained from the analysis of COHERENT CsI (2017) and LAr data extracted from [9, 10].

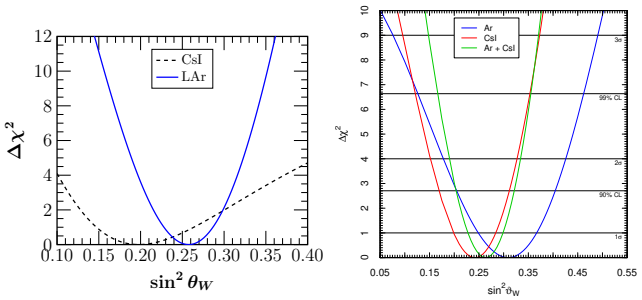

FIGURE 1: $\Delta\chi^2$ profile for $\sin^2\theta_W$ obtained from the analysis of COHERENT CsI (2017) and LAr data from [9, 10].

The 1σ result obtained using the Dresden-II reactor data is shown in Figure 2 assuming a modified Lindhard and iron-filter quenching factor models, together with the RGE running calculated in the $\overline{\text{MS}}$ renormalization scheme [11]. As already mentioned, the Dresden-II result is strongly dependent on the quenching factor model, and especially for the modified Lindhard, still affected by a large uncertainty. See [12] for more details.

2.2. New Neutrino Interactions: Light Vector Mediator

Given the rather low recoil energy threshold of the Dresden-II reactor experiment, one can expect that better sensitivities are achievable to new interactions mediated by light particles. This is the case for instance of NGI [13, 14, 15] with light mediators. The differential cross section induced by the simultaneous presence of multiple NGI interactions can be adapted to the light mediator case as [12]

$$\left.\frac{d\sigma}{dE_r}\right|_{\text{NGI}} = \frac{G_F^2}{2\pi} m_N F^2\left(q^2\right) \times \left[\zeta_S^2 \frac{2E_r}{E_r^{\max}} + \zeta_V^2\left(2 - \frac{2E_r}{E_r^{\max}}\right) + \zeta_T^2\left(2 - \frac{E_r}{E_r^{\max}}\right)\right]. \quad (3)$$

We show in Figure 3 (upper row) the extracted sensitivity on the light vector mediator scenario, at 1, 2, and 3 σ. The left

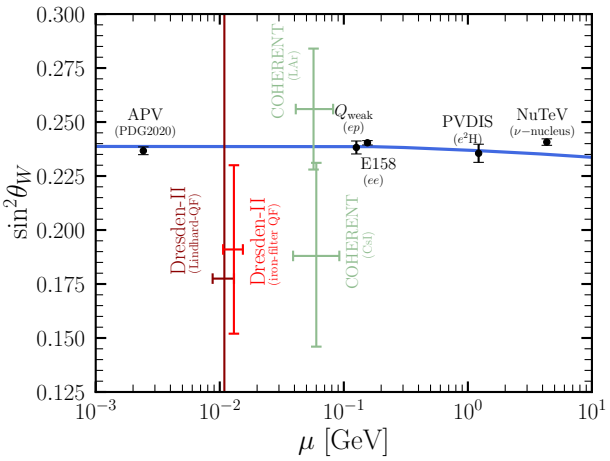

FIGURE 2: Weak mixing angle RGE running in the SM, calculated in the $\overline{\text{MS}}$ renormalization scheme as obtained in [11], along with measurements at different renormalization scales. Figure from [12].

(right) panel is obtained using the modified Lindhard (iron-filter) QF. We assume universal quark couplings and switch off the pseudovector couplings. As can be seen, at the 1σ level and above, large portions of parameter space are ruled out. At the 1 and 2σ levels, two "islands" in the region of noneffective interactions ($m_V \gtrsim 10\,\text{MeV}$) appear, due to destructive interference of the new vector contribution with the SM one. Constraints from other CEνNS experiments CONUS [16], CONNIE [17], and COHERENT CsI+LAr [18] are shown for comparison. Although not shown in the figures not to overload them, bounds from the DM experiments XENONnT [20] and LZ [21] also apply [19], and they improve upon the Dresden-II result only below $m_V \lesssim 0.2\,\text{MeV}$. (See also [22, 23, 24] for similar light mediator analyses.)

2.3. New Neutrino Interactions: Light Scalar Mediator

Next, we present in Figure 3 (medium row) the 1, 2, and 3 σ exclusion regions assuming a light scalar mediator. In this case, we focus only on the scalar interaction in equation (3), turning off the pseudoscalar couplings.

The presence of a light scalar mediator leads to smaller deviations from the data, compared to the vector case. Indeed, the scalar coupling contributes to the CEνNS cross section quadratically, whereas the vector contributes linearly, because of its interference with the SM contribution. As a consequence, the obtained limits are slightly less stringent than in the vector case. Moreover, the scalar interaction does not interfere sizeably with the SM. Similar to the vector case, bounds [19] from the DM experiments XENONnT [20] and LZ [21] apply and improve upon the Dresden-II result only below $m_S \lesssim 0.2\,\text{MeV}$.

2.4. Sterile Neutrino Dipole Portal

CEνNS can also probe nontrivial neutrino electromagnetic properties. We consider, for example, the case of a transition of an active neutrino to a massive sterile state, induced by a magnetic coupling: $\nu_L + N \to F_4 + N$. In such a scenario, the scattering process induced by an ingoing active neutrino produces a sterile neutrino in the final state. The mass of the out-

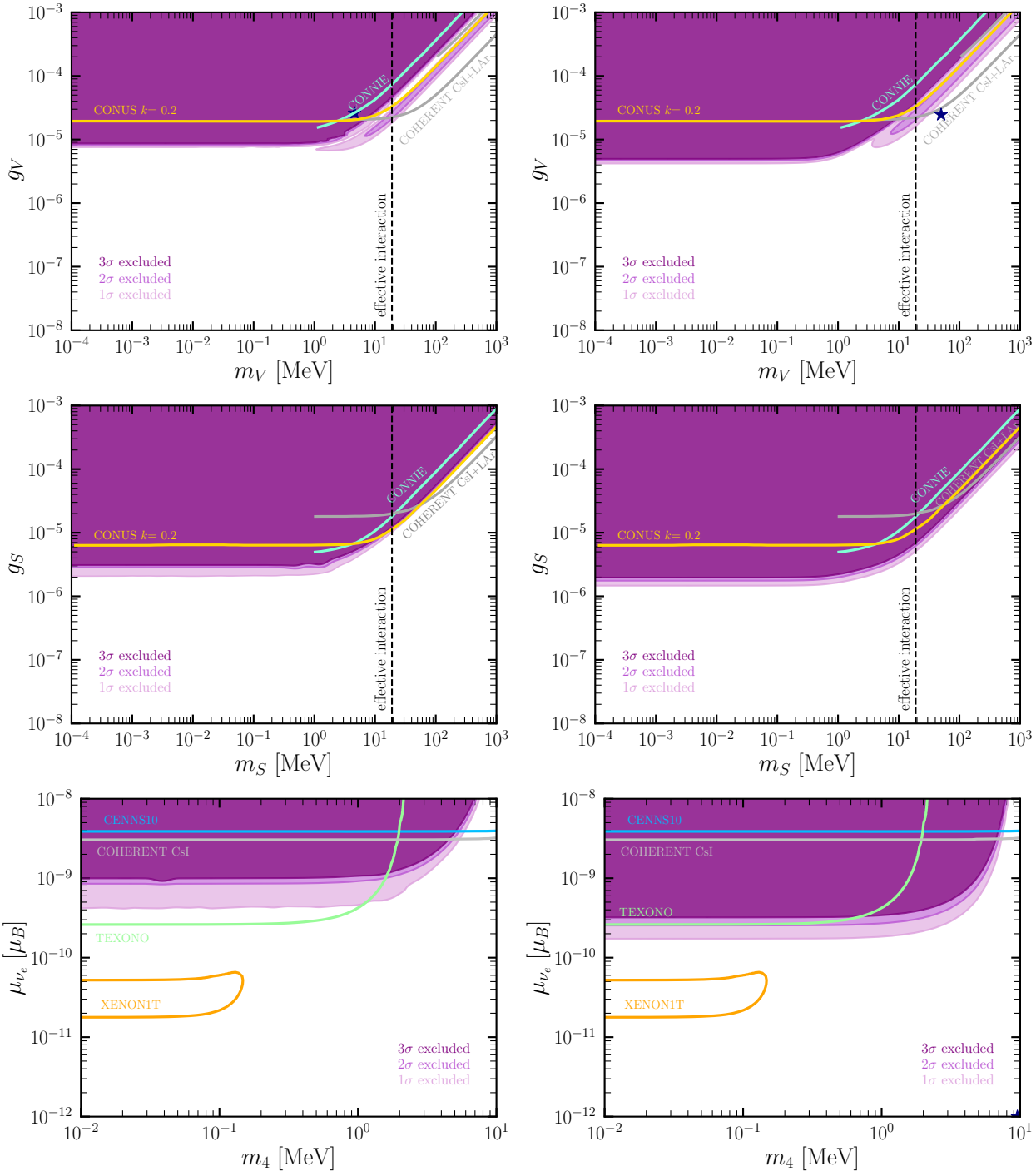

FIGURE 3: Constraints on vector NGI (upper row), scalar NGI (central row), and sterile neutrino dipole portal (lower row) in the coupling-mass plane, obtained using the modified Lindhard QF (left column) and the iron-filter QF (right column). In all panels, purple regions indicate exclusion limits at 1, 2, and 3 σ. Where present, dark blue stars specify the best-fit solutions. Figure from [12].

going fermion is constrained only by kinematic criteria: $m_4^2 \lesssim 2m_N E_r(\sqrt{\frac{2}{m_N E_r}}E_\nu - 1)$ ($m_4 \lesssim 8\,\mathrm{MeV}$ for the Dresden-II experiment). This process will contribute to the CEνNS cross section [25] through

$$\left.\frac{d\sigma}{dE_r}\right|_{\mathrm{DP}} = \alpha_{\mathrm{EM}}\mu_{\nu,\mathrm{Eff}}^2 F^2\left(q^2\right) Z^2 \left[\frac{1}{E_r} - \frac{1}{E_\nu} + \frac{m_4^4\left(E_r - m_N\right)}{8E_\nu^2 E_r^2 m_N^2} - \frac{m_4^2}{2E_\nu E_r m_N}\left(1 - \frac{E_r}{2E_\nu} + \frac{m_N}{2E_\nu}\right)\right]. \quad (4)$$

In this expression, α_{EM} refers to the electromagnetic fine structure constant and $\mu_{\nu,\mathrm{Eff}}$ to a dimensionless parameter normalized to the Bohr magneton, $\mu_B = e/(2m_e)$.

The 1, 2, and 3 σ results for this case are shown in Figure 3 (lower row), obtained assuming a modified Lindhard and iron-filter QFs. These results are competitive with the constraints from XENON1T data (indeed more constraining if one focuses only on the nuclear recoil channel) and stronger than those derived from CENNS10, while comparable to those from TEXONO. Note that the sterile neutrino dipole portal and NGI results are less sensitive to the choice of the QF model, in contrast to those found for the weak mixing angle.

3. CEνNS IMPACT ON DM DISCOVERY LIMITS

One of the most considered hypotheses to explain DM is that of being a thermal species weakly coupled to the thermal bath and whose abundance is determined by thermal freeze-out (a species usually referred to as WIMP). If this is the case, and if these WIMPs interact with the SM particles, then we may try to detect them. One of the strategies envisaged at this scope is its *direct detection* in laboratory experiments, looking for energy deposited within a detector by the DM-nuclei scattering. There is an intense DM direct detection program currently ongoing, and many experiments have already ruled out a large region in the WIMP-nucleon spin-independent cross section - WIMP mass parameter space. Some examples probing the WIMP mass range around ~0.1–1 TeV are the liquid xenon experiments LUX, PandaX-II, and XENON1T [26, 27, 28] and the liquid argon experiments DarkSide-50 and DEAP-3600 [29, 30]. The current highest sensitivity to spin-independent WIMP-nucleon scattering for masses $\gtrsim$9 GeV has been set recently by LZ [21]. In the near future, improvements in the detectors technology will allow experiments like DARWIN [31] and ARGO [32] to lower their energy thresholds and reduce the backgrounds so as to allow to set even more stringent limits or, ideally, lead to a discovery. Nonetheless, there is an important background arising from astrophysical neutrinos, from the Sun, atmosphere, and supernovae which are expected to soon constitute a limitation for these DM direct detection facilities. These neutrino backgrounds induce CEνNS and so produce nuclear recoil spectra, which, depending on the WIMP parameter space, can have a strong degeneracy with those expected from spin-independent WIMP interactions.

As shown in Figure 4, an (almost) full degeneracy is found between ^{8}B solar (atmospheric) neutrinos and a WIMP model

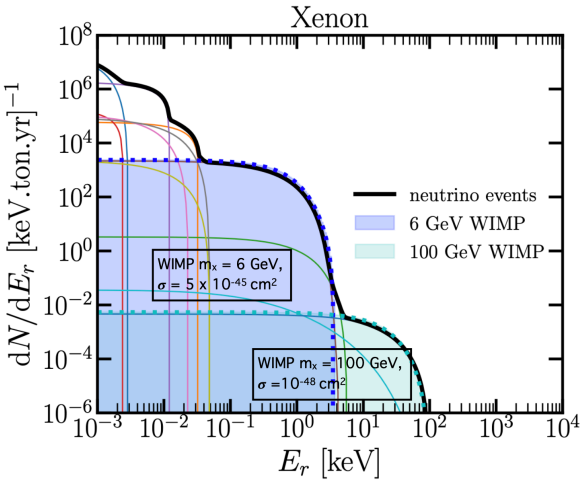

FIGURE 4: Neutrino and WIMP differential recoil spectra.

defined by a WIMP mass $m_\chi \simeq 6\,\mathrm{GeV}$ and a WIMP-nucleon cross section $\sigma_{n-\chi} \simeq 5\times10^{-45}\,\mathrm{cm}^2$ ($m_\chi \simeq 100\,\mathrm{GeV}$ and $\sigma_{n-\chi} \simeq 10^{-48}\,\mathrm{cm}^2$) [33]. This level of degeneracy thus leads to a saturation of the WIMP-nucleon cross section to which a particular experiment can have access. As a consequence, increasing the exposure of DM direct detection experiments does not imply a linear improvement of sensitivities but rather a saturation of their discovery limit [35], typically referred to as *neutrino floor* (or rather a "fog" [36]). The experimental reach of next-generation DM direct detection experiments thus depends crucially on the precision with which WIMP and CEνNS induced events can be predicted. WIMP event rates are subject to astrophysical uncertainties, while the neutrino rates depend mainly on not only neutrino flux uncertainties but also nuclear physics uncertainties and the possible existence of new interactions or mediators. Also, the *neutrino floor* should not be seen as a hard limit, as in principle it could be overcome with different techniques, including measurements of the WIMP and neutrino recoil spectra tails, directionality, measurements with different material targets, and annual modulation [37, 38, 39, 40]. However, although feasible in principle, some of them require large exposures and/or further technological improvements.

3.1. WIMP Discovery Limits

We comment here on the statistical procedure usually adopted for the determination of WIMP discovery limits, which follows a frequentist significance test using a likelihood ratio as a test statistic [41]. In full generality, both the calculation of the signal (WIMP) and background (CEνNS) events may involve nuisance parameters. We consider them only in the latter, assuming that they originate from uncertainties on the normalization of neutrino fluxes alone or combined with measured CEνNS cross section uncertainties and weak mixing angle uncertainties. A WIMP *discovery limit* is defined as the smallest WIMP cross section for which a given experiment has a 90% probability of detecting a WIMP signal at $\gtrsim 3\sigma$, or, equivalently, for which 90% of experiments have a WIMP signal above 3σ (not to be confused with the 90% CL upper limits set by the experimental collaborations).

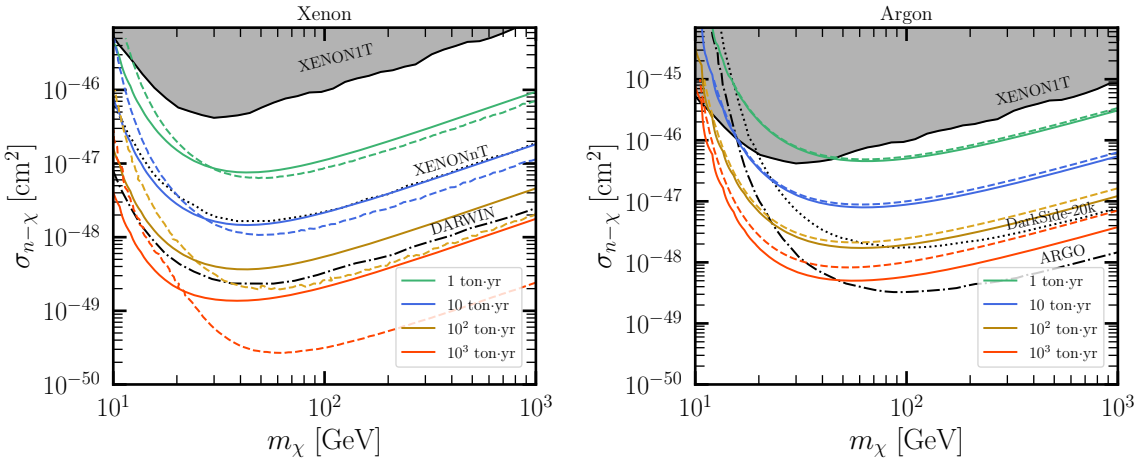

FIGURE 5: WIMP discovery limits obtained using the CEνNS cross section measurements at COHERENT with the CsI (left panel) and LAr (right panel) detectors [3, 5] (dashed curves). In addition to the nuisance parameters due to uncertainties on the neutrino flux normalizations, the results include bin-dependent nuisance parameters associated with the CEνNS cross section uncertainty. The current constraint set by XENON1T is shown in both panels. Moreover, we show as for comparison future sensitivities expected at LXe experiments XENONnT and DARWIN and at LAr experiments DarkSide-20k and ARGO. Figure from [34].

The general likelihood function depends on WIMP parameters (mass, m_χ and WIMP-nucleon cross section, $\sigma_{n-\chi}$) as well as on the nuisance parameters associated with neutrino fluxes normalization factors (denoted ϕ_α) and nuisance $\mathcal{P}$, with $\mathcal{P} = \{n_\sigma, \Theta\}$ (Θ refers to the $\sin^2\theta_W$ nuisance parameter, while n_σ stands for the ratio between the experimentally measured CEνNS cross section and its SM theoretical value):

$$\mathcal{L}\left(m_\chi, \sigma_{\chi-n}, \Phi, \mathcal{P}\right) = \prod_{i=1}^{n_{\rm bins}} P\left(N^i_{\rm Exp}, N^i_{\rm Obs}\right) G\left(\mathcal{P}_i, \mu_{\mathcal{P}_i}, \sigma_{\mathcal{P}_i}\right) \times \prod_{\alpha=1}^{n_\nu} G\left(\phi_\alpha, \mu_\alpha, \sigma_\alpha\right), \quad (5)$$

with $\Phi = (\phi_1, \ldots, \phi_{n_\nu})$. $P(x,n)$ and $G(x,\mu,\sigma)$ are Poisson and Gaussian probability distribution functions, respectively.

To set discovery limits, a null hypothesis H_0 (CEνNS background only) and an alternative hypothesis H_1—which involves the WIMP signal plus the CEνNS background—are defined. The profile likelihood ratio corresponds to a test against the null hypothesis H_0 versus the alternative hypothesis H_1.

3.2. *Data-Driven Analysis*

We first adapt a data-driven approach [34], to account for all possible uncertainties the cross section can involve, in a model-independent way. We extract from the COHERENT CsI and LAr data the CEνNS cross section central values with their standard deviations. At this scope, we weigh the theoretical SM value of the CEνNS differential cross section with a multiplicative factor n_σ and use a spectral χ^2 test to fit n_σ in each recoil energy bin. With this determination of the uncertainties on the CEνNS cross section from COHERENT data, we then compute the WIMP discovery limits.

The results are displayed in Figure 5, using CsI (LAr) data in the upper (lower) panel. In the analysis with CsI data, WIMP discovery limits improve, in general, compared with the SM expectation (solid lines). The reason is that the measured CEνNS cross section (central values) is smaller than the SM expectation, in most of the energy bins, thus resulting in a background depletion which becomes more visible with increasing exposure. Results derived using the LAr data[1] show instead the opposite behavior.

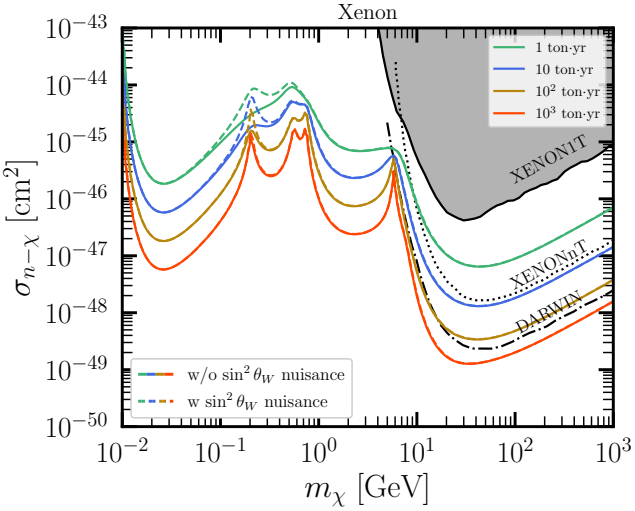

FIGURE 6: WIMP discovery limits calculated by considering uncertainties on the weak mixing angle at low energies. Results are presented for four different exposures and are compared with results obtained solely by considering neutrino flux uncertainties (solid curves). Figure from [34].

3.3. *Impact of the Weak Mixing Angle Uncertainty*

Measurements of the weak mixing angle at low energy scales ($\sim$100 MeV) involve uncertainties of the order of $\sim$10%, thus still allowing variations of the weak mixing angle value that can have an impact on WIMP discovery limits. We show in Figure 6 the discovery limits obtained by taking the $\sin^2\theta_W$ central

[1] CsI data are directly applicable to xenon since both nuclides have about the same average mass and atomic numbers.

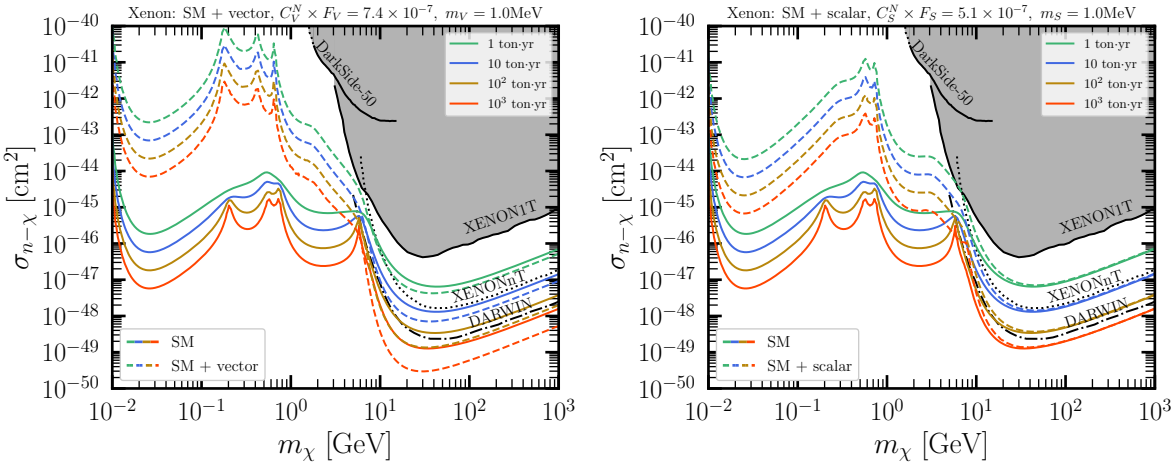

FIGURE 7: Left: WIMP discovery limit in the presence of a long-range vector interaction calculated for four different exposures and for values of the coupling and vector boson mass fixed to maximize its effect. Along with the result (dashed curves), the SM discovery limits (solid curves) are shown for comparison. Right: same as for the left graph but for a long-range scalar interaction. Couplings and masses have been fixed as required by COHERENT CsI data [42]; they correspond to the 90% CL upper bounds. Figure from [34].

value and allowing for a 10% uncertainty, combined with neutrino flux normalization and weak mixing angle uncertainties.

The effect of the weak mixing angle uncertainty is visible at low WIMP masses. The region where sizeable deviations from the "standard" result are more pronounced corresponds to those where the pp, ^{7}Be (two lines), and ^{13}N solar neutrino fluxes dominate the background. Once less abundant neutrino fluxes become relevant, the discovery limit converges to the "standard" result. The reason is the combination of a small effect and low statistics.

3.4. New Neutrino Interactions

As we have discussed previously, the CEνNS differential cross follows may be modified by the presence of a new vector lepton flavor-conserving interaction. In order to maximize the effects implied by the new interaction, we fix the new coupling to the maximum allowed value according to COHERENT CsI data at $m_V = 1$ MeV [42]. We then calculate the WIMP discovery limit, this time assuming only the nuisance parameters associated with neutrino flux normalization factors. Similarly, also a scalar interaction in both the effective and light regime can affect the CEνNS background from astrophysical neutrinos. In this case, since the scalar coupling involves a chirality flip, it cannot (sizeably) interfere with the SM contribution, in contrast to the vector interaction. We present the results of the impact of these new interactions on WIMP discovery limits in Figure 7. In the vector mediator case, at low WIMP masses, the discovery limit is diminished by several orders of magnitude. At low momentum transfer, the new contribution is enhanced and overcomes the SM contribution, as the CEνNS cross section is enhanced toward low momentum transfer regions. Consequently, the neutrino background increases dramatically. For regions above 10 GeV, after the ^{8}B and hep neutrino fluxes reach their kinematic tail, the discovery limit improves. The reason for this change in the behavior is due to the fact that the SM coherent weak charge is negative, while the new contribution is positive. So, as q^2 increases, the new contribution becomes less prominent and destructively interferes with the SM term.

The scalar contribution also peaks toward the low momentum transfer region (low WIMP mass region), thus enhancing the background and worsening the discovery limit. The effect is, however, less pronounced than in the vector case, since the leading vector term is linear in the coupling while the scalar contributes quadratically. At high momentum transfer (high WIMP mass), the scalar keeps enhancing the background because destructive interference with the SM is not possible.

4. CONCLUSIONS

In this talk, we have discussed the physics potential of the CEνNS process, in both the SM and beyond. First, we have presented the main features of CEνNS, a process in which neutrinos scatter on a nucleus which acts as a single particle. In particular, we have highlighted the coherency condition leading to a substantial enhancement of the cross section ($\propto N^2$). Then, we have listed some of the CEνNS extended physics potential, including SM tests (determination of the weak mixing angle at low momentum transfer), solar and supernova neutrinos, new interactions, sterile neutrinos, and nuclear properties. We have presented results addressing some of these possible applications, from analyses of recent data from the COHERENT and the Dresden-II experiments. In the second part of the talk, we have reconsidered possible variations of the neutrino floor, exploiting the measurements of the CEνNS process by the COHERENT collaboration.

To conclude, we want to stress that we can expect a wealth of information from forthcoming CEνNS data. These will have important implications for both precision tests of the SM and for probing new physics.

CONFLICTS OF INTEREST

The author declares that there are no conflicts of interest regarding the publication of this paper.

ACKNOWLEDGMENTS

V. De Romeri acknowledges financial support by the SEJI/2020/016 grant (Generalitat Valenciana) and by the Spanish grant PID2020-113775GB-I00 (AEI/10.13039/501100011033).

References

[1] D. Z. Freedman. "Coherent Neutrino Nucleus Scattering as a Probe of the Weak Neutral Current," Phys. Rev. D **9**, 1389–1392 (1974) doi:10.1103/PhysRevD.9.1389.

[2] V. B. Kopeliovich and L. L. Frankfurt. "Isotopic and chiral structure of neutral current," JETP Lett. **19**, 145–147 (1974).

[3] D. Akimov et al. [COHERENT]. "Observation of Coherent Elastic Neutrino-Nucleus Scattering," Science **357**, no. 6356, 1123–1126 (2017), doi:10.1126/science.aao0990 [arXiv:1708.01294 [nucl-ex]].

[4] D. Akimov et al. [COHERENT]. "Measurement of the Coherent Elastic Neutrino-Nucleus Scattering Cross Section on CsI by COHERENT," Phys. Rev. Lett. **129**, no. 8, 081801 (2022), doi:10.1103/PhysRevLett.129.081801 [arXiv:2110.07730 [hep-ex]].

[5] D. Akimov et al. [COHERENT]. "First Measurement of Coherent Elastic Neutrino-Nucleus Scattering on Argon," Phys. Rev. Lett. **126**, no. 1, 012002 (2021), doi:10.1103/PhysRevLett.126.012002 [arXiv:2003.10630 [nucl-ex]].

[6] J. Colaresi, J. I. Collar, T. W. Hossbach, A. R. L. Kavner, C. M. Lewis, A. E. Robinson, and K. M. Yocum. "First results from a search for coherent elastic neutrino-nucleus scattering at a reactor site," Phys. Rev. D **104**, no. 7, 072003 (2021), doi:10.1103/PhysRevD.104.072003 [arXiv:2108.02880 [hep-ex]].

[7] J. Colaresi, J. I. Collar, T. W. Hossbach, C. M. Lewis, and K. M. Yocum. "Suggestive evidence for Coherent Elastic Neutrino-Nucleus Scattering from reactor antineutrinos," [arXiv:2202.09672 [hep-ex]].

[8] M. Abdullah, H. Abele, D. Akimov, G. Angloher, D. Aristizabal Sierra, C. Augier, A. B. Balantekin, L. Balogh, P. S. Barbeau and L. Baudis et al. "Coherent elastic neutrino-nucleus scattering: Terrestrial and astrophysical applications," [arXiv:2203.07361 [hep-ph]].

[9] O. G. Miranda, D. K. Papoulias, G. Sanchez Garcia, O. Sanders, M. Tórtola, and J. W. F. Valle. "Implications of the first detection of coherent elastic neutrino-nucleus scattering (CEvNS) with Liquid Argon," JHEP **05**, 130 (2020) [erratum: JHEP **01**, 067 (2021)], doi:10.1007/JHEP05(2020)130 [arXiv:2003.12050 [hep-ph]].

[10] M. Cadeddu, F. Dordei, C. Giunti, Y. F. Li, E. Picciau, and Y. Y. Zhang. "Physics results from the first COHERENT observation of coherent elastic neutrino-nucleus scattering in argon and their combination with cesium-iodide data," Phys. Rev. D **102**, no. 1, 015030 (2020), doi:10.1103/PhysRevD.102.015030 [arXiv:2005.01645 [hep-ph]].

[11] J. Erler and M. J. Ramsey-Musolf. "The Weak mixing angle at low energies," Phys. Rev. D **72**, 073003 (2005), doi:10.1103/PhysRevD.72.073003 [arXiv:hep-ph/0409169 [hep-ph]].

[12] D. Aristizabal Sierra, V. De Romeri, and D. K. Papoulias. "Consequences of the Dresden-II reactor data for the weak mixing angle and new physics," JHEP **09**, 076 (2022), doi:10.1007/JHEP09(2022)076 [arXiv:2203.02414 [hep-ph]].

[13] D. Aristizabal Sierra, V. De Romeri, and N. Rojas. "COHERENT analysis of neutrino generalized interactions," Phys. Rev. D **98**, 075018 (2018), doi:10.1103/PhysRevD.98.075018 [arXiv:1806.07424 [hep-ph]].

[14] T. D. Lee and C. N. Yang. "Question of Parity Conservation in Weak Interactions," Phys. Rev. **104**, 254–258 (1956), doi:10.1103/PhysRev.104.254.

[15] M. Lindner, W. Rodejohann, and X. J. Xu, "Coherent Neutrino-Nucleus Scattering and new Neutrino Interactions," JHEP **03**, 097 (2017), doi:10.1007/JHEP03(2017)097 [arXiv:1612.04150 [hep-ph]].

[16] H. Bonet et al. [CONUS]. "Novel constraints on neutrino physics beyond the standard model from the CONUS experiment," JHEP **05**, 085 (2022), doi:10.1007/JHEP05(2022)085 [arXiv:2110.02174 [hep-ph]].

[17] A. Aguilar-Arevalo et al. [CONNIE]. "Search for light mediators in the low-energy data of the CONNIE reactor neutrino experiment," JHEP **04**, 054 (2020), doi:10.1007/JHEP04(2020)054 [arXiv:1910.04951 [hep-ex]].

[18] M. Atzori Corona, M. Cadeddu, N. Cargioli, F. Dordei, C. Giunti, Y. F. Li, E. Picciau, C. A. Ternes, and Y. Y. Zhang. "Probing light mediators and $(g-2)_\mu$ through detection of coherent elastic neutrino nucleus scattering at COHERENT," JHEP **05**, 109 (2022), doi:10.1007/JHEP05(2022)109 [arXiv:2202.11002 [hep-ph]].

[19] S. K. A., A. Majumdar, D. K. Papoulias, H. Prajapati, and R. Srivastava. "First results of LZ and XENONnT: A comparative study of neutrino properties and light mediators," [arXiv:2208.06415 [hep-ph]].

[20] E. Aprile et al. [(XENON Collaboration)†† and XENON]. "Search for New Physics in Electronic Recoil Data from XENONnT," Phys. Rev. Lett. **129** (2022) no. 16, 161805, doi:10.1103/PhysRevLett.129.161805 [arXiv:2207.11330 [hep-ex]].

[21] J. Aalbers et al. [LZ]. "First Dark Matter Search Results from the LUX-ZEPLIN (LZ) Experiment," [arXiv:2207.03764 [hep-ex]].

[22] J. Liao, H. Liu, and D. Marfatia. "Implications of the first evidence for coherent elastic scattering of reactor neutrinos," Phys. Rev. D **106**, no. 3, L031702 (2022), doi:10.1103/PhysRevD.106.L031702 [arXiv:2202.10622 [hep-ph]].

[23] P. Coloma, I. Esteban, M. C. Gonzalez-Garcia, L. Larizgoitia, F. Monrabal, and S. Palomares-Ruiz, "Bounds on new physics with data of the Dresden-II reactor experiment and COHERENT," JHEP **05**, 037 (2022), doi:10.1007/JHEP05(2022)037 [arXiv:2202.10829 [hep-ph]].

[24] A. Majumdar, D. K. Papoulias, R. Srivastava, and J. W. F. Valle, "Physics implications of recent Dresden-II reactor data," [arXiv:2208.13262 [hep-ph]].

[25] D. McKeen and M. Pospelov. "Muon Capture Constraints on Sterile Neutrino Properties," Phys. Rev. D **82**, 113018 (2010), doi:10.1103/PhysRevD.82.113018 [arXiv:1011.3046 [hep-ph]].

[26] D. S. Akerib et al. [LUX]. "Results from a search for dark matter in the complete LUX exposure," Phys. Rev. Lett. **118** (2017) no. 2, 021303, doi:10.1103/PhysRevLett.118.021303 [arXiv:1608.07648 [astro-ph.CO]].

[27] Y. Meng et al. [PandaX-4T]. "Dark Matter Search Results from the PandaX-4T Commissioning Run," Phys. Rev. Lett. **127** (2021) no. 26, 261802, doi:10.1103/PhysRevLett.127.261802 [arXiv:2107.13438 [hep-ex]].

[28] E. Aprile et al. [XENON]. "Dark Matter Search Results from a One Ton-Year Exposure of XENON1T," Phys. Rev. Lett. **121** (2018) no. 11, 111302, doi:10.1103/PhysRevLett.121.111302 [arXiv:1805.12562 [astro-ph.CO]].

[29] P. Agnes et al. [DarkSide]. "DarkSide-50 532-day Dark Matter Search with Low-Radioactivity Argon," Phys. Rev. D **98** (2018) no. 10, 102006, doi:10.1103/PhysRevD.98.102006 [arXiv:1802.07198 [astro-ph.CO]].

[30] R. Ajaj et al. [DEAP]. "Search for dark matter with a 231-day exposure of liquid argon using DEAP-3600 at SNOLAB," Phys. Rev. D **100** (2019) no. 2, 022004, doi:10.1103/PhysRevD.100.022004 [arXiv:1902.04048 [astro-ph.CO]].

[31] J. Aalbers et al. [DARWIN]. "DARWIN: towards the ultimate dark matter detector," JCAP **11** (2016), 017, doi:10.1088/1475-7516/2016/11/017 [arXiv:1606.07001 [astro-ph.IM]].

[32] J. Billard, M. Boulay, S. Cebrián, L. Covi, G. Fiorillo, A. Green, J. Kopp, B. Majorovits, K. Palladino and F. Petricca et al. "Direct detection of dark matter—APPEC committee report*," Rept. Prog. Phys. **85** (2022) no. 5, 056201, doi:10.1088/1361-6633/ac5754 [arXiv:2104.07634 [hep-ex]].

[33] J. Billard, L. Strigari, and E. Figueroa-Feliciano. Phys. Rev. D **89**, no. 2, 023524 (2014), doi:10.1103/PhysRevD.89.023524 [arXiv:1307.5458 [hep-ph]].

[34] D. Aristizabal Sierra, V. De Romeri, L. J. Flores, and D. K. Papoulias. "Impact of COHERENT measurements, cross section uncertainties and new interactions on the neutrino floor," JCAP **01**, no. 01, 055 (2022), doi:10.1088/1475-7516/2022/01/055 [arXiv:2109.03247 [hep-ph]].

[35] L. E. Strigari. "Neutrino Coherent Scattering Rates at Direct Dark Matter Detectors," New J. Phys. **11**, 105011 (2009), doi:10.1088/1367-2630/11/10/105011 [arXiv:0903.3630 [astro-ph.CO]].

[36] C. A. J. O'Hare. "New Definition of the Neutrino Floor for Direct Dark Matter Searches," Phys. Rev. Lett. **127**, no. 25, 251802 (2021), doi:10.1103/PhysRevLett.127.251802 [arXiv:2109.03116 [hep-ph]].

[37] J. Aalbers, K. Abe, V. Aerne, F. Agostini, S. A. Maouloud, D. S. Akerib, D. Y. Akimov, J. Akshat, A. K. A. Musalhi and F. Alder et al. "A Next-Generation Liquid Xenon Observatory for Dark Matter and Neutrino Physics," [arXiv:2203.02309 [physics.ins-det]].

[38] Y. Zhuang, L. E. Strigari, and R. F. Lang, "Time variation of the atmospheric neutrino flux at dark matter detectors," Phys. Rev. D **105** (2022) no. 4, 043001, doi:10.1103/PhysRevD.105.043001 [arXiv:2110.14723 [hep-ph]].

[39] C. A. J. O'Hare. "Can we overcome the neutrino floor at high masses?," Phys. Rev. D **102** (2020) no. 6, 063024, doi:10.1103/PhysRevD.102.063024 [arXiv:2002.07499 [astro-ph.CO]].

[40] C. A. J. O'Hare, D. Loomba, K. Altenmuller, H. Alvarez-Pol, F. D. Amaro, H. M. Araujo, D. Aristizabal Sierra, J. Asaadi, D. Attie and S. Aune et al. "Recoil imaging for dark matter, neutrinos, and physics beyond the Standard Model," [arXiv:2203.05914 [physics.ins-det]].

[41] G. Cowan, K. Cranmer, E. Gross, and O. Vitells, "Asymptotic formulae for likelihood-based tests of new physics," Eur. Phys. J. C **71**, 1554 (2011) [erratum: Eur. Phys. J. C **73**, 2501 (2013)], doi:10.1140/epjc/s10052-011-1554-0 [arXiv:1007.1727 [physics.data-an]].

[42] D. Aristizabal Sierra, B. Dutta, S. Liao, and L. E. Strigari, "Coherent elastic neutrino-nucleus scattering in multi-ton scale dark matter experiments: Classification of vector and scalar interactions new physics signals," JHEP **12**, 124 (2019), doi:10.1007/JHEP12(2019)124 [arXiv:1910.12437 [hep-ph]].